CHEMISTRY OF MATERIALS
Article

Chem. Mater. **2009,** *21,* 3655–3661 3655
DOI:10.1021/cm901150c

Chemical Synthesis of Two-Dimensional Iron Chalcogenide Nanosheets: FeSe, FeTe, Fe(Se,Te), and $FeTe_2$

Karl D. Oyler,[†] Xianglin Ke,[‡] Ian T. Sines,[†] Peter Schiffer,[‡,§] and Raymond E. Schaak*[,†,§]

[†]*Department of Chemistry and* [‡]*Department of Physics and* [§]*Materials Research Institute, The Pennsylvania State University, University Park, Pennsylvania 16802*

Received April 25, 2009. Revised Manuscript Received June 14, 2009

Transition metal chalcogenides are important materials because of their range of useful properties and applications, including as thermoelectrics, magnetic semiconductors, superconductors, quantum dots, sensors, and photovoltaics. In particular, iron chalcogenides have received renewed attention following the discovery of superconductivity in PbO-type β-FeSe and related solid solutions. This paper reports a low-temperature solution chemistry route to the synthesis of β-FeSe, β-FeTe, $FeTe_2$, and several members of the β-Fe(Se,Te) solid solution. The samples were analyzed by powder XRD, TEM, EDS, SAED, SEM with elemental mapping, AFM, and SQUID magnetometry. Consistent with the layered crystal structures, the FeSe, FeTe, and Fe(Se,Te) products are predominantly two-dimensional single-crystal nanosheets with thicknesses of approximately 2−3 nm and edge lengths ranging from 200 nm to several micrometers. $FeTe_2$ forms a mixture of nanosheets and one-dimensional sheet-derived nanostructures. None of the samples are superconducting, which could be due to size effects, nonstoichiometry, or low-level impurities.

Introduction

Transition metal chalcogenides represent an important family of materials that have proven useful as thermoelectrics,[1,2] magnetic semiconductors,[3] superconductors,[4,5] quantum dots,[6,7] sensors,[8] and photovoltaics.[9−11] Iron chalcogenides in particular have been targeted for their interesting magnetic properties, including for their potential use in magnetic semiconducting and spintronic applications.[12−14] Iron selenides, tellurides, and their solid solutions have recently received renewed attention following the unexpected discovery of superconductivity in β-FeSe,[15] where β-FeSe refers to the tetragonal PbO-type phase (*P*4/*nmm*) and α-FeSe corresponds to the hexagonal NiAs-type phase ($P6_3/mmc$) based on the conventional assignment.[16] Superconductivity has also been observed in related systems such as solid solutions of Fe(Se,Te)[17] and Fe(S,Te).[18] For example, PbO-type β-FeSe is superconducting with a critical temperature (T_c) of 8 K, which can be increased up to 27 K under high pressure.[19] Atomic substitution was also found to increase the T_c to 15 and 10 K in similarly structured $FeSe_{0.5}Te_{0.5}$[17] and $FeTe_{0.8}S_{0.2}$[18] solid solutions, respectively.

β-FeSe and related iron chalcogenides are typically synthesized at temperatures in excess of 700 °C, often involving heating times of several days, using traditional powder metallurgical methods,[15,16,19] flux growth,[20] or vapor self-transport.[21] Other methods such as chemical

*Corresponding author. E-mail: schaak@chem.psu.edu.

(1) Wood, C. *Rep. Prog. Phys.* **1988**, *51*(4), 459–539.
(2) Poudel, B.; Hao, Q.; Ma, Y.; Lan, Y. C.; Minnich, A.; Yu, B.; Yan, X.; Wang, D. Z.; Muto, A.; Vashaee, D.; Chen, X. Y.; Liu, J. M.; Dresselhaus, M. S.; Chen, G.; Ren, Z. *Science* **2008**, *320*(5876), 634–638.
(3) Dietl, T. *Semicond. Sci. Technol.* **2002**, *17*(4), 377–392.
(4) Fischer, Ø. *Appl. Phys.* **1978**, *16*(1), 1–28.
(5) Niu, H. J.; Hampshire, D. P. *Phys. Rev. B* **2004**, *69*(17), 9.
(6) Murray, C. B.; Norris, D. J.; Bawendi, M. G. *J. Am. Chem. Soc.* **1993**, *115*(19), 8706–8715.
(7) Malik, M. A.; Revaprasadu, N.; O'Brien, P. *Chem. Mater.* **2001**, *13*(3), 913–920.
(8) Schöning, M. J.; Kloock, J. P. *Electroanalysis* **2007**, *19*(19−20), 2029–2038.
(9) Ennaoui, A.; Fiechter, S.; Pettenkofer, C.; Alonsovante, N.; Buker, K.; Bronold, M.; Hopfner, C.; Tributsch, H. *Sol. Energy Mater. Sol. Cells* **1993**, *29*(4), 289–370.
(10) Huynh, W. U.; Dittmer, J. J.; Alivisatos, A. P. *Science* **2002**, *295*(5564), 2425–2427.
(11) Mitzi, D. B.; Yuan, M.; Liu, W.; Kellock, A. J.; Chey, S. J.; Deline, V.; Schrott, A. G. *Adv. Mater.* **2008**, *20*(19), 3657–3662.
(12) Takemura, Y.; Suto, H.; Honda, N.; Kakuno, K.; Saito, K. *J. Appl. Phys.* **1997**, *81*(8), 5177–5179.
(13) Wu, X. J.; Zhang, Z. Z.; Zhang, J. Y.; Ju, Z. G.; Li, B. H.; Li, B. S.; Shan, C. X.; Zhao, D. X.; Yao, B.; Shen, D. Z. *Thin Solid Films* **2008**, *516*(18), 6116–6119.
(14) Wu, X. J.; Zhang, Z. Z.; Zhang, J. Y.; Li, B. H.; Ju, Z. G.; Lu, Y. M.; Li, B. S.; Shen, D. Z. *J. Appl. Phys.* **2008**, *103*(11), 113501.
(15) Hsu, F. C.; Luo, J. Y.; Yeh, K. W.; Chen, T. K.; Huang, T. W.; Wu, P. M.; Lee, Y. C.; Huang, Y. L.; Chu, Y. Y.; Yan, D. C.; Wu, M. K. *Proc. Natl. Acad. Sci. U.S.A.* **2008**, *105*(38), 14262–14264.
(16) McQueen, T. M.; Huang, Q.; Ksenofontov, V.; Felser, C.; Xu, Q.; Zandbergen, H.; Hor, Y. S.; Allred, J.; Williams, A. J.; Qu, D.; Checkelsky, J.; Ong, N. P.; Cava, R. J. *Phys. Rev. B* **2009**, *79*(1), 014522.
(17) Yeh, K. W.; Huang, T. W.; Huang, Y. L.; Chen, T. K.; Hsu, F. C.; Wu, P. M.; Lee, Y. C.; Chu, Y. Y.; Chen, C. L.; Luo, J. Y.; Yan, D. C.; Wu, M. K. *EPL* **2008**, *84*, 37002.
(18) Mizuguchi, Y.; Tomioka, F.; Tsuda, S.; Yamaguchi, T.; Takano, Y. *Appl. Phys. Lett.* **2009**, *94*, 012503.
(19) Mizuguchi, Y.; Tomioka, F.; Tsuda, S.; Yamaguchi, T.; Takano, Y. *Appl. Phys. Lett.* **2008**, *93*(15), 152505.
(20) Zhang, S. B.; Sun, Y. P.; Zhu, X. D.; Zhu, X. B.; Swang, B.; Lei, H.; Luo, X.; Yang, Z. R.; Song, W. H.; Dai, J. M. *Supercond. Sci. Technol.* **2009**, *22*(1), 4.
(21) Patel, U.; Hua, J.; Yu, S. H.; Avci, S.; Xiao, Z. L.; Claus, H.; Schlueter, J.; Vlasko-Vlasov, V. V.; Welp, U.; Kwok, W. K. *Appl. Phys. Lett.* **2009**, *94*(8), 3.

Published on Web 07/10/2009

vapor deposition (CVD)[13,22] and molecular beam epitaxy (MBE)[12] have been used to fabricate thin films. As nanoscale materials, core−shell nanofibers of carbon-coated β-FeSe have been reported,[23] and $FeSe_2$[24−27] and $FeTe_2$[26−29] nanoparticles have been obtained using solution-based solvothermal reduction. Other nanocrystalline iron sulfide and selenide phases have also been made, including FeS_2,[30] Fe_7S_8,[27,31] and impure samples of NiAs-type α-FeSe.[32] However, there have been no reports of a low-temperature solution-based chemical route to PbO-type β-FeSe, as well as some of the related iron chalcogenides. Such a synthetic capability for these materials is important for several reasons. For example, interesting size-dependent phenomena have been discovered for other superconductors when synthetic routes produced size and dimensionality control.[33−36] Also, low-temperature chemical routes can allow for the stabilization of nonequilibrium polymorphs,[37,38] possibly leading to the discovery of new superconductors or magnetic materials in these and related systems.

Here we report a low-temperature solution chemistry method for the synthesis of PbO-type β-FeSe, as well as the tellurides β-FeTe and $FeTe_2$. A Fe(Se,Te) solid solution with tunable composition could also be prepared. Importantly, this synthetic method yields predominantly two-dimensional single-crystal nanosheets. Morphologically similar lamellar nanostructures have proven pivotal for solution-based processing,[11,39] thin film formation,[40−42] enhancing physical properties,[43,44] and discovering new physical phenomena for diverse classes of materials that include graphene,[45] layered metal oxides[46,47] and sulfides,[44,48−50] silicate clays,[43,51,52] and layered double hydroxides.[53,54] Although the chemically synthesized iron chalcogenide nanosheets do not show evidence of superconductivity, they represent a timely addition to the extensive library of two-dimensional nanocrystal systems[43−54] and could serve as a starting point for exploring interesting dimension-dependent properties because of their size, crystallinity, and anisotropic morphology.

Experimental Section

Materials. All chemicals were used as received and stored in an Ar-atmosphere glovebox. Iron pentacarbonyl (99.5%), hexadecylamine (HDA), tellurium powder (99.99%, −325 mesh) and selenium powder (99+%) were purchased from Alfa-Aesar. Trioctylphosphine (TOP) and trioctylphosphine oxide (TOPO) were obtained from Aldrich and were of technical-grade purity. All syntheses were set up in an Ar-atmosphere glovebox and carried out under Ar using standard Schlenk techniques; workups were performed in air.

Synthesis. *β-FeSe.* HDA (3.38 g) and TOPO (6.19 g) were added to a three-neck round-bottom flask equipped with a reflux condenser, thermometer adapter, rubber septum, and vacuum adapter. The mixture was heated to 160 °C at which point a solution of $Fe(CO)_5$ (0.27 mL, d = 1.49 g/mL) and Se powder (0.316 g) dissolved in 3 mL of TOP was injected. The solution was heated to 250 °C for 1 h and observed to darken to black indicating the formation of nanoparticles. The reaction mixture was allowed to cool to 80 °C, at which point it was poured into an equal volume of 3:1 hexane/ethanol. The mixture was centrifuged to isolate a dark precipitate from an transparent brown-colored supernatant which was washed with additional fractions of 3:1 hexane/ethanol until the supernatant became clear. The product was additionally washed with ∼20 mL of dichloromethane to remove residual TOP and then dried under vacuum.

β-FeTe and $FeTe_2$ (Frohbergite). The reaction conditions and workup were identical to the FeSe case. To synthesize FeTe, 0.013 g of Te powder was substituted for Se along with 0.27 mL of $Fe(CO)_5$ (it was found that a 20:1 excess of Fe to Te was required for the FeTe to form without $FeTe_2$ impurities). Pure $FeTe_2$ could be obtained from a larger amount of Te (0.256 g), also with 0.27 mL of $Fe(CO)_5$.

(22) Feng, Q. J.; Shen, D. Z.; Zhang, J. Y.; Li, B. S.; Li, B. H.; Lu, Y. M.; Fan, X. W.; Liang, H. W. *Appl. Phys. Lett.* **2006**, *88*(1), 012505.
(23) Pol, S. V.; Pol, V. G.; Gedanken, A. *J. Phys. Chem. C* **2007**, *111*(45), 16781–16786.
(24) Han, Z. H.; Li, Y. P.; Lu, J.; Yu, S. H.; Zhao, H. Q.; Qian, Y. T. *Mater. Res. Bull.* **2000**, *35*(11), 1825–1829.
(25) Yang, J.; Cheng, G. H.; Zeng, J. H.; Yu, S. H.; Liu, X. M.; Qian, Y. T. *Chem. Mater.* **2001**, *13*(3), 848–853.
(26) Liu, A. P.; Chen, X. Y.; Zhang, Z. J.; Jiang, Y.; Shi, C. W. *Solid State Commun.* **2006**, *138*(10−11), 538–541.
(27) Xie, Y.; Zhu, L. Y.; Jiang, X. C.; Lu, J.; Zheng, X. W.; He, W.; Li, Y. Z. *Chem. Mater.* **2001**, *13*(11), 3927–3932.
(28) Zhang, W. X.; Yang, Z. H.; Zhan, J. H.; Yang, L.; Yu, W. C.; Zhou, G. E.; Qian, Y. T. *Mater. Lett.* **2001**, *47*(6), 367–370.
(29) Zhang, J. H.; Wu, B.; O'Connor, C. J.; Simmons, W. B. *J. Appl. Phys.* **1993**, *73*(10), 5718–5720.
(30) Qian, X. F.; Xie, Y.; Qian, Y. T. *Mater. Lett.* **2001**, *48*(2), 109–111.
(31) Kong, X.; Lou, T.; Li, Y. *J. Alloys Compd.* **2005**, *390*, 236–239.
(32) Campos, C. E. M.; de Lima, J. C.; Grandi, T. A.; Machado, K. D.; Pizani, P. S. *Solid State Commun.* **2002**, *123*(3−4), 179–184.
(33) Tian, M. L.; Wang, J. G.; Snyder, J.; Kurtz, J.; Liu, Y.; Schiffer, P.; Mallouk, T. E.; Chan, M. H. W. *Appl. Phys. Lett.* **2003**, *83*(8), 1620–1622.
(34) Tian, M. L.; Wang, J. G.; Kumar, N.; Han, T. H.; Kobayashi, Y.; Liu, Y.; Mallouk, T. E.; Chan, M. H. W. *Nano Lett.* **2006**, *6*(12), 2773–2780.
(35) Wu, F. Y.; Yang, C. C.; Wu, C. M.; Wang, C. W.; Li, W. H. *J. Appl. Phys.* **2007**, *101*(9), 09G111.
(36) Chou, N. H.; Ke, X.; Schiffer, P.; Schaak, R. E. *J. Am. Chem. Soc.* **2008**, *130*(26), 8140–8141.
(37) Vasquez, Y.; Luo, Z. P.; Schaak, R. E. *J. Am. Chem. Soc.* **2008**, *130* (36), 11866–11867.
(38) Dawood, F.; Schaak, R. E. *J. Am. Chem. Soc.* **2009**, *131*(2), 424–425.
(39) Mitzi, D. B.; Kosbar, L. L.; Murray, C. E.; Copel, M.; Afzali, A. *Nature* **2004**, *428*(6980), 299–303.
(40) Schaak, R. E.; Mallouk, T. E. *Chem. Mater.* **2002**, *14*(4), 1455–1471.
(41) Kleinfeld, E. R.; Ferguson, G. S. *Science* **1994**, *265*(5170), 370–373.
(42) Rouse, J. H.; MacNeill, B. A.; Ferguson, G. S. *Chem. Mater.* **2000**, *12*(8), 2502–2507.
(43) Giannelis, E. P. *Adv. Mater.* **1996**, *8*(1), 29–35.
(44) Seo, J. W.; Jun, Y. W.; Park, S. W.; Nah, H.; Moon, T.; Park, B.; Kim, J. G.; Kim, Y. J.; Cheon, J. *Angew. Chem., Int. Ed.* **2007**, *46* (46), 8828–8831.
(45) Geim, A. K.; Novoselov, K. S. *Nat. Mater.* **2007**, *6*(3), 183–191.
(46) Schaak, R. E.; Mallouk, T. E. *Chem. Mater.* **2000**, *12*(9), 2513–2516.
(47) Saupe, G. B.; Waraksa, C. C.; Kim, H. N.; Han, Y. J.; Kaschak, D. M.; Skinner, D. M.; Mallouk, T. E. *Chem. Mater.* **2000**, *12*(6), 1556–1562.
(48) Novoselov, K. S.; Jiang, D.; Schedin, F.; Booth, T. J.; Khotkevich, V. V.; Morozov, S. V.; Geim, A. K. *Proc. Natl. Acad. Sci. U.S.A.* **2005**, *102*(30), 10451–10453.
(49) Li, Y. D. D.; Li, X. L. L.; He, R. R. R.; Zhu, J.; Deng, Z. X. X. *J. Am. Chem. Soc.* **2002**, *124*(7), 1411–1416.
(50) Gautam, U. K.; Vivekchand, S. R. C.; Govindaraj, A.; Rao, C. N. R. *Chem. Commun.* **2005**, *31*, 3995–3997.
(51) Alexandre, M.; Dubois, P. *Mater. Sci. Eng. R-Rep.* **2000**, *28*(1−2), 1–63.
(52) Pavlidou, S.; Papaspyrides, C. D. *Prog. Polym. Sci.* **2008**, *33*(12), 1119–1198.
(53) Leroux, F.; Besse, J. P. *Chem. Mater.* **2001**, *13*(10), 3507–3515.
(54) Liu, Z. P.; Ma, R. Z.; Ebina, Y.; Iyi, N.; Takada, K.; Sasaki, T. *Langmuir* **2007**, *23*(2), 861–867.

β-Fe(Se,Te) Solid Solutions. The reaction conditions and workup were also identical to the FeSe case, the only difference being the additional presence of Te powder along with Se. $FeSe_{0.67}Te_{0.33}$ was formed from a 10:1 Se/Te precursor ratio using 0.158 g of Se and 0.026 g of Te. $FeSe_{0.62}Te_{0.38}$ was formed from a 7.5:1 precursor ratio using 0.118 g of Se and 0.026 g of Te. $FeSe_{0.57}Te_{0.43}$ was formed from a 5:1 precursor ratio using 0.079 g of Se and 0.026 g of Te.

Characterization. Powder X-ray diffraction (XRD) data were collected by a Bruker Advance D8 X-ray diffractometer using Cu Kα radiation. Rietveld refinement of the XRD data was carried out using TOPAS, and lattice parameters were determined using Chekcell. Transmission electron microscopy (TEM) images and selected area electron diffraction (SAED) patterns were obtained from a JEOL 1200 EX II operating at 80 kV or from a JEOL JEM-2010 LaB_6 microscope operating at 200 kV. $FeTe_2$ samples for microtoming were prepared using Spurr's Kit from Electron Microscopy Sciences. The sample was embedded by suspension in a 1:1 resin/acetone mixture and left to stand for 90 min before decanting the supernatant. A 1:3 resin/acetone mixture was then added, mixed, allowed to stand for 120 min, and then decanted. Finally, pure resin was added, mixed, and allowed to harden overnight in a 60 °C oven. The solid resin was microtomed into thin sheets and pressed onto Formvar-coated copper TEM grids for imaging. Scanning electron microscopy (SEM) and energy-dispersive X-ray spectroscopy (EDS) data were acquired from a FEI Quanta 200 Environmental SEM. Magnetization measurements were taken by a Quantum Design Superconducting Quantum Interference Device (SQUID) magnetometer with an applied field of 50 Oe.

Atomic force microscopy (AFM) data were collected by a Dimension Instruments 3100 atomic force microscope equipped with PPP-NCHR tapping mode AFM tips from Nanosensors. To prepare samples, a ~1 cm^2 fragment of single-crystal Si wafer was cleaned by submersion in a beaker of RCA-1 solution for 20 min. The silicon fragment was rinsed with nanopure water and then immersed face down at a ~45° angle in a ~0.1 M solution of analyte in toluene for 45 min. The wafer was removed from the solution, rinsed with nanopure water, and then dried under a stream of argon.

Results and Discussion

The chosen synthetic method is very closely related to the techniques often used to synthesize II−VI semiconductor nanocrystals such as CdSe and CdTe,[6,55,56] for example, the reaction of zerovalent precursors which decompose in a high-boiling solvent. For the iron chalcogenides, $Fe(CO)_5$ and Se/Te-TOP (TOP = trioctylphosphine) were used as elemental precursors, and hexadecylamine (HDA) and trioctylphosphine oxide (TOPO) were used as the solvent system. As a representative example, the reaction of $Fe(CO)_5$ with Se-TOP in HDA and TOPO at 250 °C (see Experimental Section for details) yielded β-FeSe. Powder XRD data (Figure 1) verify the phase formation and purity of β-FeSe: the experimental pattern matches well with the simulated data, and no other crystalline impurity peaks are observed. The lattice parameters, *a* and *c*, were determined to be 3.7689(37) and 5.5067(4) Å, respectively, and are very close to reported literature values for bulk β-FeSe (a = 3.765 and c = 5.518 Å).[57] Additionally, Rietveld structure refinement of the powder XRD pattern determined the composition of the material to be $Fe_{0.994(1)}Se_{1.014(1)}$, indicating a slight excess of selenium.

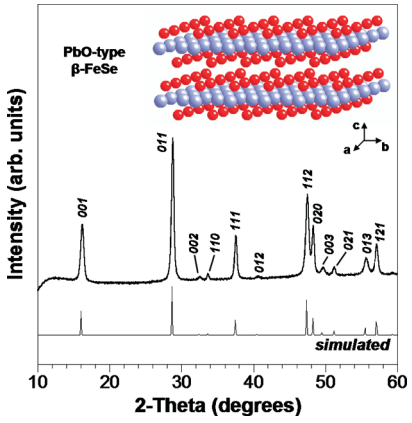

Figure 1. Experimental and simulated powder XRD patterns for β-FeSe. The tetragonal PbO-type crystal structure is shown as the inset, where the blue and red spheres represent Fe and Se, respectively.

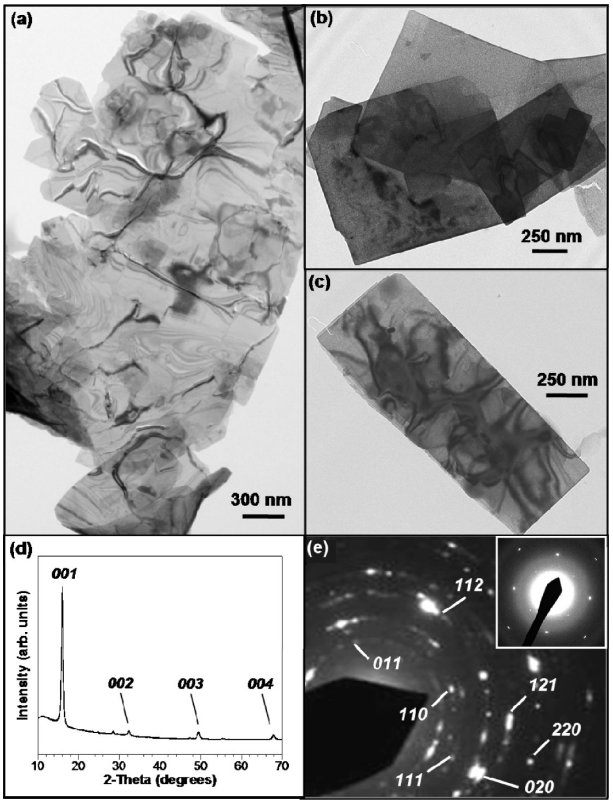

Figure 2. (a−c) TEM images of β-FeSe nanosheets. Dropcasting the nanosheets produces significant preferred orientation along [001], as shown in the XRD pattern in (d), and confirms the two-dimensional morphology. SAED patterns confirm the tetragonal PbO-type crystal structure (e), as well as the single-crystalline nature of isolated nanosheets (e, inset).

Representative TEM images (Figure 2) show that the β-FeSe products typically form thin nanosheets with edge lengths ranging from 200 nm to several micrometers,

(55) Talapin, D. V.; Rogach, A. L.; Kornowski, A.; Haase, M.; Weller, H. *Nano Lett*. **2001**, *1*(4), 207–211.
(56) Qu, L. H.; Yu, W. W.; Peng, X. P. *Nano Lett*. **2004**, *4*(3), 465–469.
(57) Hägg, G.; Kindström, A. L. *Z. Phys. Chem. B* **1933**, *22*, 453.

either as large irregular sheets (Figure 2a) or smaller rectangular plates (Figure 2b,c). The samples, in dry powder form, yield powder XRD patterns as shown in Figure 1. The XRD patterns match bulk β-FeSe because of significant aggregation of the sheets in powder form. However, the isolated nanosheets (prepared by sonication and drop-casting from toluene) produce powder XRD patterns with significant preferred orientation (Figure 2d). The 001 peak predominates, while the intensities of the 002, 003, and 004 reflections are also enhanced compared to the aggregated sample, indicating that the sheets are truncated along [001] and are essentially two-dimensional crystals that correspond to the $a-b$ plane. Selected area electron diffraction (SAED) patterns for both the large irregular sheets (Figure 2a) and the isolated nanosheets (Figure 2b,c) are consistent with the PbO-type structure of β-FeSe. Representative SAED patterns for the nanosheet aggregates and an isolated nanosheet (Figure 2e and inset, respectively) indicate the single-crystalline nature of the individual sheets and the polycrystalline character of the aggregates. A typical SEM image of the β-FeSe product (Figure 3a) shows aggregates composed of two-dimensional sheets, further confirming the nanosheet morphology. EDS mapping data for Fe and Se (Figure 3b,c, respectively) along with the combined overlay (Figure 3d) confirm the uniform distribution of both elements across the sample.

The AFM image in Figure 4a shows the topography of the β-FeSe sheets, which are largely flat with small bumps that are consistent with the polymer adhesion layer that coats the Si surface. A line scan through one of the sheets (Figure 4b) indicates an average thickness of approximately 1.5−2.0 nm. A single layer of the β-FeSe structure, which corresponds to the height of the unit cell, is approximately 0.55 nm. This indicates that the β-FeSe nanosheets are generally 2−3 unit cells thick.

The formation of two-dimensional nanosheets can be rationalized by the crystal structure and the preferred orientation direction observed by powder XRD. The PbO-type structure of β-FeSe contains layers of covalently bonded Fe and Se. These layers are held together through van der Waals forces and stack vertically along the c-axis of the crystal structure (Figure 1, inset). When β-FeSe begins to form in solution, the coordinating solvent binds to the selenium layers, truncating growth along the [001] direction and supporting growth within the $a-b$ plane to form two-dimensional nanosheets. Similar mechanisms have been proposed for chemically related alloys such as Bi_2Te_3[58,59] and Sb_2Te_3[60] synthesized using solvent-based approaches. Control experiments conducted in weakly coordinating solvents such as diphenyl ether did not lead to the formation of nanosheets (Figure S1, Supporting Information), also lending support to this surfactant-directed hypothesis.

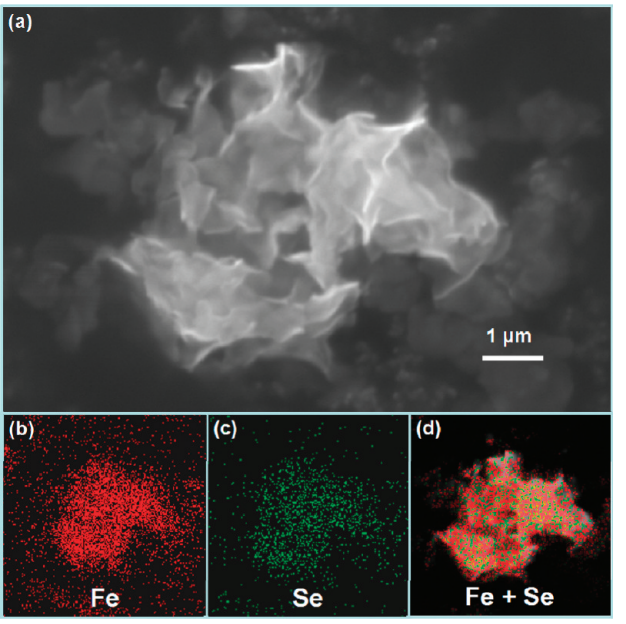

Figure 3. (a) SEM image of β-FeSe nanosheet clusters with associated elemental mapping data showing the (b) Fe and (c) Se along with (d) combined Fe and Se regions, indicating uniform distribution of both elements throughout the nanosheet cluster.

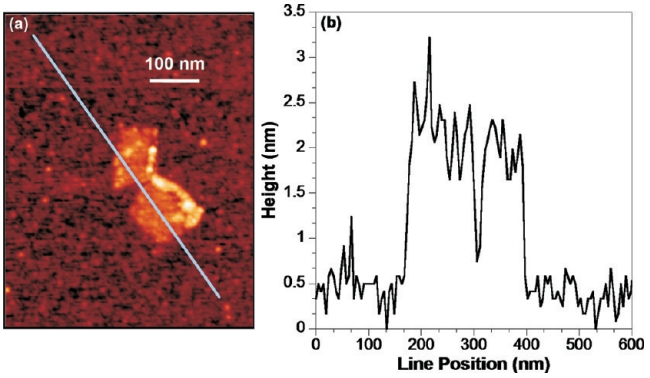

Figure 4. (a) AFM image of an isolated β-FeSe nanosheet and (b) line scan corresponding to the blue line in (a).

When Se-TOP is substituted with Te-TOP, nanosheets of PbO-type β-FeTe form (a 20:1 molar excess of the Fe precursor to the Te-TOP was required to avoid the formation of crystalline $FeTe_2$ impurities). The powder XRD pattern in Figure 5a confirms that the crystalline product corresponds to phase-pure β-FeTe. The lattice constants, a and c, were found to be 3.8220(3) and 6.2704 (2) Å, respectively, which match the literature values for bulk β-FeTe (a = 3.821 and c = 6.269 Å).[61] Figure 5b,c shows representative TEM images of the β-FeTe products, and the SAED pattern in Figure 5a (inset) confirms the phase assignment. Like β-FeSe, thin nanosheets comprise a majority of the samples, with some nanosheet aggregates also present.

When the Fe:Te precursor ratio is changed to 1:1, anisotropic nanocrystals of frohbergite-type $FeTe_2$ form

(58) Lu, W. G.; Ding, Y.; Chen, Y. X.; Wang, Z. L.; Fang, J. Y. *J. Am. Chem. Soc.* **2005**, *127*(28), 10112–10116.
(59) Zhang, G. Q.; Wang, W.; Lu, X. L.; Li, X. G. *Cryst. Growth Des.* **2009**, *9*(1), 145–150.
(60) Wang, W. Z.; Poudel, B.; Yang, J.; Wang, D. Z.; Ren, Z. F. *J. Am. Chem. Soc.* **2005**, *127*(40), 13792–13793.
(61) Finlayson, D. M.; Grieg, G.; Llewellyn, J. P.; Smith, T. *Proc. Phys. Soc., B* **1956**, *69*, 860–862.

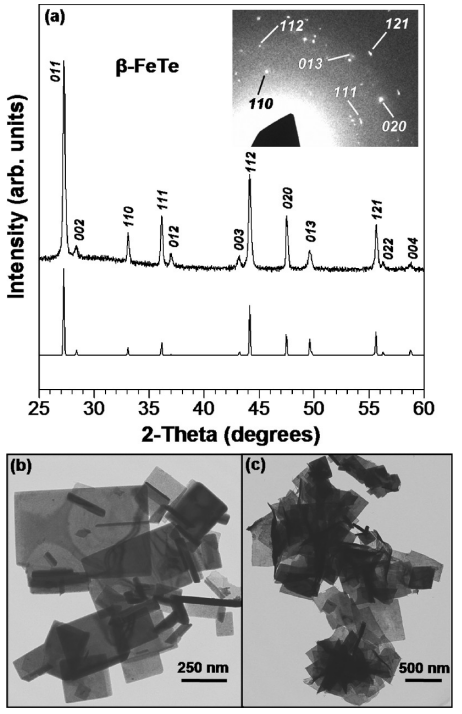

Figure 5. (a) Powder XRD pattern and SAED pattern (inset) of β-FeTe. TEM images highlight the nanosheet morphology, both as (b) isolated rectangular sheets or (c) agglomerates of nanosheets.

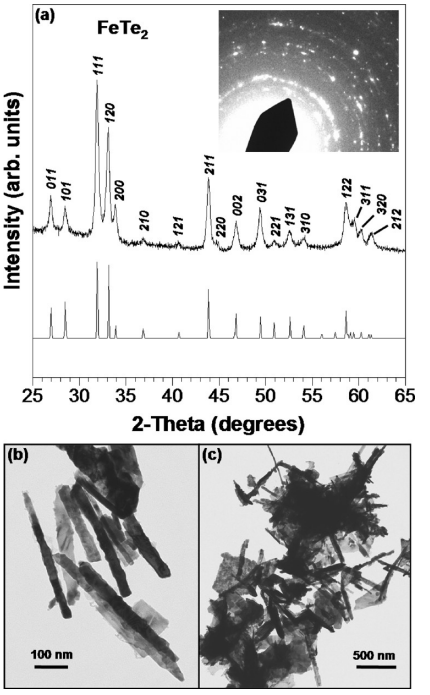

Figure 6. (a) Powder XRD pattern and SAED pattern (inset) of $FeTe_2$. TEM images showing one-dimensional nanostructures (b), with evidence of lamellar intermediates (c).

(Figure 6). The powder XRD data in Figure 6a confirm the formation of $FeTe_2$, as does the SAED pattern. The $FeTe_2$ system forms predominantly one-dimensional nanostructures instead of sheets (Figure 6b,c). Higher-resolution TEM images show evidence for sheets that emanate from the one-dimensional nanostructures (Figure 6c and Supporting Information Figure S3), implying that sheets may form initially and roll into tight bundles, in analogy to other oxide and chalcogenide materials that form nanoscrolls.[47,49,62−64] The cross-sectional TEM image in Figure S3 (Supporting Information) further supports this hypothesis, showing evidence of hollow tubes (e.g., nanoscrolls) upon slicing the sample during microtoming. Although the crystal structure of $FeTe_2$ is different from that of PbO-type β-FeSe and β-FeTe, there are still alternating regions of Fe and Te. The coordinating solvent would still be expected to preferentially bind to the Te regions, helping to template two-dimensional nanostructures.

In bulk β-FeSe, substitution of Te to form a Fe(Se,Te) solid solution has been reported to increase the superconducting T_c. Fe(Se,Te) can also be obtained using this solution chemistry method, as confirmed by the powder XRD pattern of a Fe(Se,Te) solid solution member in Figure 7a. Comparing this pattern to those of FeSe and FeTe (reproduced in Figure 7a), the peak positions of the solid solution appear intermediate to the positions of the equivalent reflections in the two end members. The slightly broader peak widths observed for the solid solution is likely the result of some substitutional disorder throughout the sample. The average stoichiometry of the solid solution members can be tuned simply by varying the molar ratios of the Se-TOP and Te-TOP precursors, as shown by the powder XRD patterns (Figure 7b) for several members of the Fe(Se,Te) solid solution. Figure 7c highlights a representative peak shift of the 011 reflection that is consistent with lattice expansion associated with the progressive incorporation of the larger Te atoms into the β-FeSe lattice. EDS data indicate that the solid solution members with nominal (starting) compositions of 10:1, 7.5:1, and 5:1 have actual compositions of $FeSe_{0.67}Te_{0.33}$, $FeSe_{0.62}Te_{0.38}$, and $FeSe_{0.57}Te_{0.43}$, respectively, normalized to Fe(Se,Te) with Se + Te = 1 and with errors of approximately ± 0.02 for each value. This is roughly consistent with the compositions expected from Vegard's law (considering unit cell volume), which corroborates the XRD and EDS data. Excess Fe was observed by EDS, suggesting the possible presence of amorphous iron oxide impurities (no crystalline impurities were found by XRD or SAED). It is worth noting that the actual Te:Se ratio in the solid solution products is greater than the nominal stoichiometry of the reagents, suggesting a preference for the incorporation of Te into the structure relative to Se. Representative TEM images of one member of the Fe(Se,Te) solid solution, $FeSe_xTe_{1-x}$ ($x = 0.62$), are shown in Figure 8a,b, along with the SAED pattern in Figure 8c confirming that it is a single PbO-type phase. A representative SEM image of bulk quantities of the $x = 0.57$ solid solution nanosheets is shown in Figure 9. The associated elemental mapping data for Fe (Figure 9b),

(62) Schaak, R. E.; Mallouk, T. E. *Chem. Mater.* **2000**, *12*(11), 3427–3434.
(63) Kobayashi, Y.; Hata, H.; Salama, M.; Mallouk, T. E. *Nano Lett.* **2007**, *7*(7), 2142–2145.
(64) Shi, L.; Xu, Y. M.; Li, Q. *Cryst. Growth Des.* **2008**, *8*(10), 3521–3525.

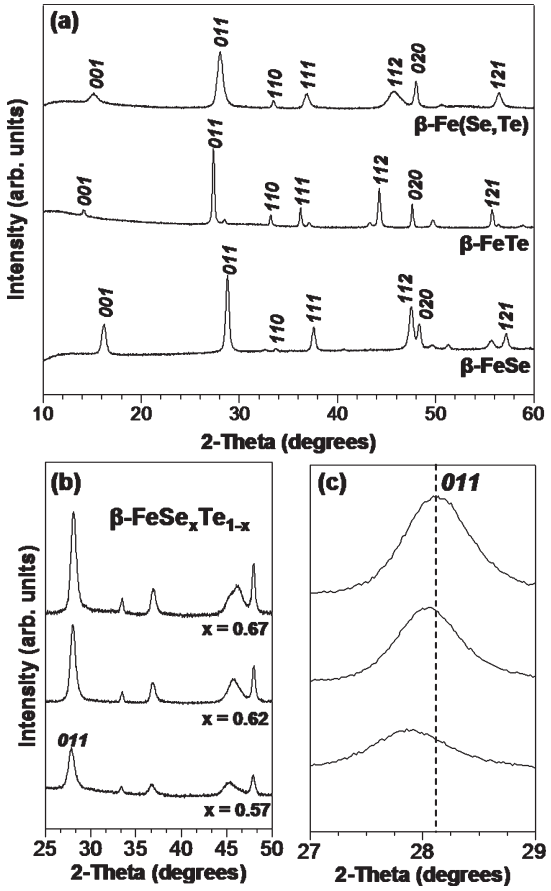

Figure 7. (a) Powder XRD patterns comparing a solid solution of Fe(Se,Te) to end members FeSe and FeTe. (b) Powder XRD patterns of a series of β-FeSe$_x$Te$_{1-x}$ solid solutions, with x values of 0.67, 0.62, and 0.57 (determined by EDS). A close-up of the 011 peak (c) shows peak shifts that are consistent with the relative Te:Se ratios in the β-FeSe$_x$Te$_{1-x}$ solid solutions.

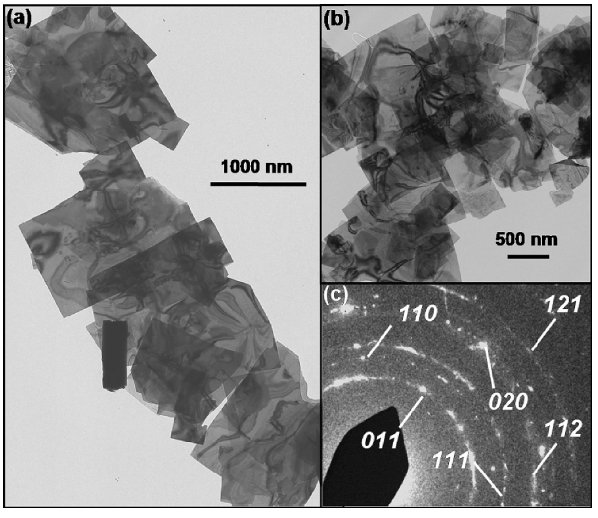

Figure 8. Representative TEM images of the $x = 0.62$ β-FeSe$_x$Te$_{1-x}$ solid solution (a, b) highlight the nanosheet morphology. The SAED pattern (c) confirms the tetragonal, PbO-type structure.

Se (Figure 9c), Te (Figure 9d), and the overlay of all three (Figure 9e) confirms the uniform distribution of all three elements throughout the sample.

Despite the high crystallinity and phase purity determined by the chemical and structural analyses, the

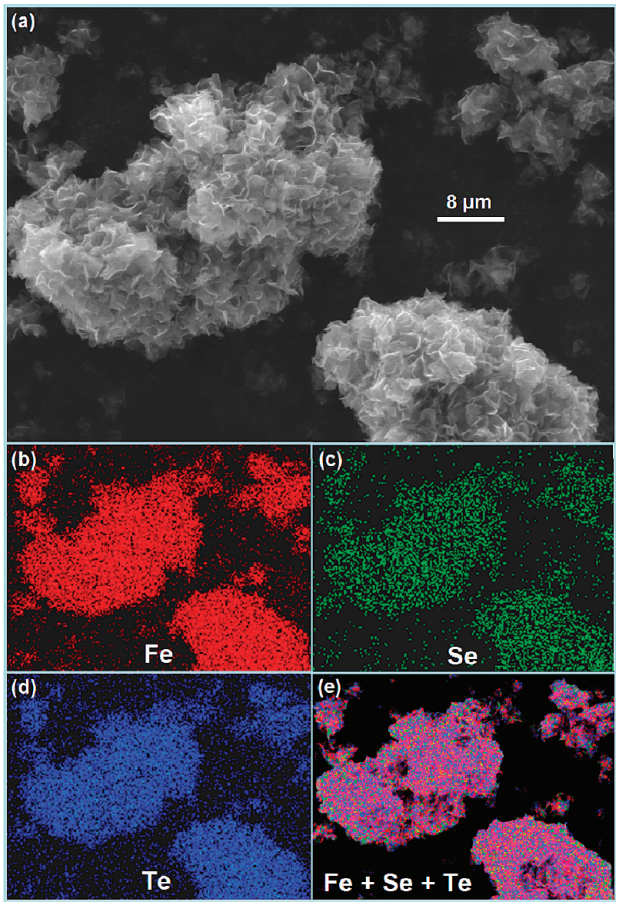

Figure 9. (a) Representative SEM image of β-FeSe$_x$Te$_{1-x}$ ($x = 0.57$) nanosheet clusters with associated elemental mapping data (b–d) showing the (b) Fe, (c) Se, and (d) Te regions of the sample. The overlapping data is shown in (e), indicating the uniform distribution of all three elements into the nanosheet clusters.

PbO-type compounds showed no evidence of a Meissner effect that would be indicative of superconductivity. Plots of magnetic susceptibility vs temperature for β-FeSe, β-FeTe, β-FeSe$_{0.62}$Te$_{0.38}$, and FeTe$_2$ are shown in Figure S2 (Supporting Information). Several features are evident, including an ordering transition at approximately 60 K that is consistent with antiferromagnetic ordering in bulk samples.[65,66] However, we cannot exclude the possibility that magnetic impurities at the level of 1% of the sample are the dominant cause of the magnetic signal. Despite this, the data clearly show that the samples are not superconducting.

There are several reasons why the lack of superconductivity in these systems is not an unexpected result. Recent studies conducted on thin films of β-FeSe deposited by pulsed laser deposition indicated that c-axis oriented films less than 140 nm thick displayed barely perceptible superconductivity.[67] This was attributed to the lack of a necessary structural distortion, which was hypothesized

(65) Sales, B. C.; Sefat, A. S.; McGuire, M. A.; Jin, R. Y.; Mandrus, D.; Mozharivskyj, Y. *Phys. Rev. B* **2009**, *79*(9), 094521.
(66) Bao, W.; Qiu, Y.; Huang, Q.; Green, M. A.; Zajdel, P.; Fitzsimmons, M. R.; Zhernenkov, M.; Fang, M.; Qian, B.; Vehstedt, E. K.; Yang, J.; Pham, H. M.; Spinu, L.; Mao, Z. Q. **2008**, arXiv:0809.2058v1 (pre-print).
(67) Wang, M. J.; Luo, J. Y.; Huang, T. W.; Chang, H. H.; Chen, T. K.; Hsu, F. C.; Wu, C. T.; Wu, P. M.; Chang, A. M.; Wu, M. K. **2009**, arXiv:0904.1858v1 (pre-print).

to be required for the occurrence of superconductivity. Our nanosheets are also oriented along the *c*-axis and are much thinner (~2 nm), which could explain the absence of superconductivity in our samples. In addition, other reports have provided evidence that superconductivity in β-FeSe is highly dependent on stoichiometry[16,68,69] and requires a slight excess of Fe for superconductivity to appear; for example, β-$Fe_{1.01}Se$ is superconducting with T_c = 8.5 K while β-$Fe_{1.03}Se$ is not superconducting.[16] Our samples of β-FeSe were determined to have a slight excess of Se ($Fe_{0.994}Se_{1.014}$), so the lack of superconductivity could also be a result of this nonideal stoichiometry. Further synthetic modifications to fine-tune the size and thickness of the nanosheets, as well as the purity, are in progress and could help to experimentally establish the thickness dependence of the superconductivity in *single-crystal* samples of β-FeSe. Likewise, measurements on single nanosheets of β-FeSe could provide a direct way of probing both dimensionality and the anisotropic nature of superconductivity in this interesting system.

Conclusions

In summary, we have reported a low-temperature solution-based synthesis of PbO-type β-FeSe, as well as related Te-containing compounds and the composition-tunable Fe(Se,Te) solid solution. Because of the crystal structure and coordinating solvent, the iron chalcogenides tend to form nanocrystals with two-dimensional single-crystal nanosheet and nanosheet-derived morphologies. Although the β-FeSe and β-Fe(Se,Te) nanosheets did not show evidence of superconductivity, these materials are still interesting for future studies, both as probes for further exploring the dependence of superconductivity on size and dimensionality and for elucidating potential magnetic properties in related systems.

Acknowledgment. This work was supported by the U.S. Department of Energy (DE-FG02-08ER46483), a DuPont Young Professor Grant, a Beckman Young Investigator Award, a Sloan Research Fellowship, and a Camille Dreyfus Teacher-Scholar Award. X.K. and P.S. thank the Penn State MRSEC (DMR-0820404) and NSF (DMR-0701582) for funding. Electron microscopy was performed at the Electron Microscopy Facility at the Huck Institute for Life Sciences and at the Penn State Materials Research Institute. The authors acknowledge use of facilities at the PSU site of the NSF NNIN and thank Dr. Tad Daniel of the Materials Research Institute for acquisition of the AFM data, as well as Zac Schaefer for assistance with XRD Rietveld refinement.

Supporting Information Available: XRD and TEM data for spherical β-FeSe nanoparticles synthesized using diphenyl ether and magnetic susceptibility data for β-FeSe, β-FeTe, β-Fe(Se, Te), and $FeTe_2$ (PDF). This material is available free of charge via the Internet at http://pubs.acs.org.

(68) Margadonna, S.; Takabayashi, Y.; McDonald, M. T.; Kasperkiewicz, K.; Mizuguchi, Y.; Takano, Y.; Fitch, A. N.; Suard, E.; Prassides, K. *Chem. Commun.* **2008**, *43*, 5607–5609.
(69) Pomjakushina, E.; Conder, K.; Pomjakushin, V.; Bendele, M.; Khasanov, R. **2009**, arXiv:0905.2115v1 (pre-print).